This is a post-peer-review, pre-copyedit version of an article published in The International Journal of Advanced Manufacturing Technology. The final authenticated version is available online at: https://doi.org/10.1007/s00170-017-0597-2

Mechatronics of a ball screw drive using a N degrees of freedom dynamic model

Igor Ansoategui[1], Francisco J. Campa[2]

[1]Mechanical Engineering Department. University College of Engineering Vitoria-Gasteiz. University of the Basque Country UPV/EHU.

[2]Mechanical Engineering Department. Bilbao Faculty of Engineering. University of the Basque Country UPV/EHU.

e-mail: igor.ansoategui@ehu.eus, fran.campa@ehu.es

Abstract

High performance position control in machine tools can only be achieved modelling the dynamic behavior of the mechatronic system composed by the motor, transmission and control during the design stage. In this work, a complex analytical model of a ball screw drive is presented and integrated in a mechatronic model of the actuator to predict the dynamic behaviour and analyze the impact of each component of the transmission. First, a simple 2 degrees of freedom model is presented, and is analysis sets the basis for the development of a more complex model of several degrees of freedom, whose resulting fundamental transfer functions are represented using natural and modal coordinates. The modeling in modal coordinates carries a reduction of the transfer function that reduces computational work. The two models are compared and experimentally validated in time and frequency domain by means of experimental tests carried out on a specifically developed ball screw drive test bench.

Keywords: Ball screw drive Machine tool dynamics Mechatronics

Nomenclature

m, J	Mass, inertia moment
c	Viscous damping
k	Stiffness
ω_i	i-thmodal frequency
ϕ_{ij}	i-thdof component of the j-th eigenvector
x, θ	Linear, angular position in natural coordinates
δ	Positionin modal coordinates
ξ_i	Damping coefficient of the i-th mode
f, τ	Force, torque in natural coordinates
g	Force in modal coordinates
K_v	Proportional gain of the position loop
K_p	Proportional gain of the velocity loop
T_i	Integral time of the velocity loop

This is a post-peer-review, pre-copyedit version of an article published in The International Journal of Advanced Manufacturing Technology. The final authenticated version is available online at: https://doi.org/10.1007/s00170-017-0597-2

1 Introduction

In order to optimize the performance of machine tool drives, a huge effort has been made in recent decades to investigate the global mechatronic behaviour through modeling [1]. The more complex or detailed the model is, the more realistic will be the simulation, if the dynamic parameters are well known, and a better design will be done. The specifications that must be guaranteed in the design stage are generally accuracy, that is, precision following the programmed tool path, robustness against perturbations as the cutting forces and acceleration and jerk to perform intricate motions. In the end, those requirements are fulfilled if a certain bandwidth is achieved in the drive. The bandwidth will depend on the mechanical properties of the drive and transmission chain but also on the control performance, so it is necessary to have a good modelling tool of both systems to assess the design stage.

However, not only a good selection of components must be made during the design. Some authors actuate on the mechanical system or control system modifying preloads or adding filtering techniques [2], [3], developing intelligent algorithms [4] or applied reinforcement learning methods [5]. Some author even add piezoelectric actuators to complement the action of the drives [6]. All this to improve the dynamic behavior of the actuation system, that is to improve the drive bandwidth while avoiding resonances.

In order to get a model that describes accurately the dynamic behavior of the drive test bench and for finding the optimal formulation, several options have been posed in the literature of the Academy. Some works focus on lumped parameters modeling with Newton [1], [7] and Lagrange [8]–[10] form. Other techniques to model dynamical systems are by numerical models of finite elements [8], [11], [12] or multibody models. As the screw shaft body stiffness is variable along its axis, some authors have formulated Lagrange equations by integral functions [9], [13]. From the equations of motion, after passing them to the frequency domain, the dynamics of the drive can be modeled by transfer functions, or use the state space approximation as [8].

A drive modeled by lumped parameters can be developed by inertial models such [5], [12], [13], and 2 dof models such as [14], [15]. So far, several authors have developed lumped parameter models in ball screw drives, generally using two dofs models. There are authors that have even developed a four dof model [4], [16] using a lumped parameter system, then analyze in more detail the different modes of vibration.

In the literature, in the case of N dof models systems have been developed using a space-state approximation such as [8], [17]. Zulaika and Altamira [18], developed a model of lumped parameters of 2 dof of a ball screw drive in modal coordinates.

In this paper it has been chosen the Newton formulation, using a lumped parameters model. In this paper a model of 2 dof and another of N dof in natural and modal coordinates are developed. The model in modal coordinates will present equations for transfer functions in a more explicit way, and isolating the drive with as many lumped parameters as possible will interpret the dynamic behavior of the system in a more realistic and precise way. A comparison between 2 dof and N dof models is made, and especially the advantages of the modal coordinates for the N dof models will be explained.

This is a post-peer-review, pre-copyedit version of an article published in The International Journal of Advanced Manufacturing Technology. The final authenticated version is available online at: https://doi.org/10.1007/s00170-017-0597-2

This paper is organized as follows. Section 2 develops the mechatronic model of the drive both using a 2 dof and a 7 dof dynamic model in natural and modal coordinates. In Section 3, the modelling is applied to a ball screw drive. In Section 4, an experimental validation with a test bench is presented comparing the model and the experimental data in time and frequency domain. The paper will end with some conclusions in Section 5.

2 Mechatronic model of a ball screw drive

In Fig.1 it is shown the ball screw test bench that has been modeled and tested. It has a Fagor FKM 42.30A servomotor with a rated torque of 6.3 Nm, a Korta KBS-3210ball screw with single nut and flange with an outer diameter of 32 mm and a pitch of 10 mm, and a Heidenhain Ls186 MI640optical linear encoder with a resolution of 0.5 µm.A pneumatic cylinder can impose a force on the table, simulating a feed disturbance. The drive is controlled by a CNC Fagor 8035, with has an oscilloscope function that allows measuring internal signals, as the position at the motor encoder and linear encoder, the following error or the motor torque and intensity.

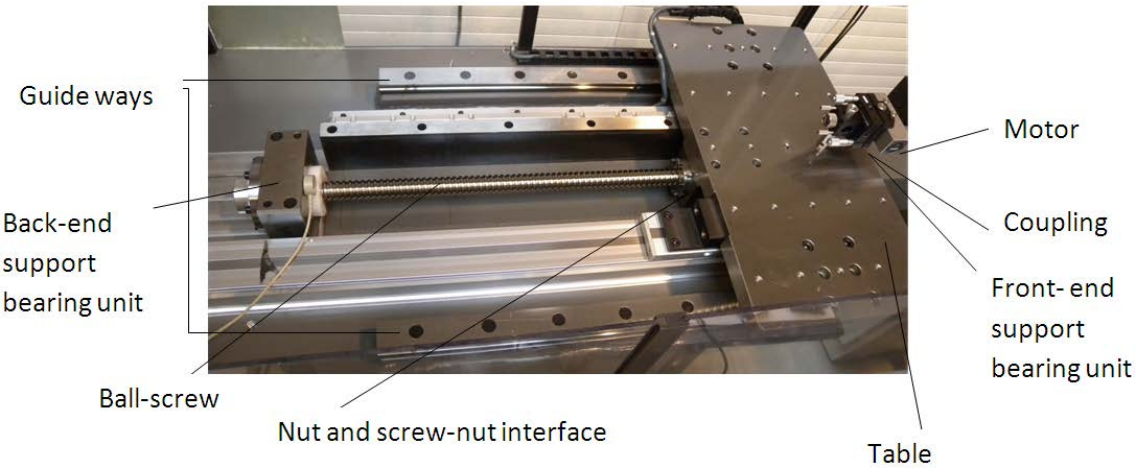

Fig. 1 Ballscrew drive testbench.

To analyze the dynamic behavior of the drive, a mechatronic model has been developed in Matlab/Simulink, see Fig.2. Regarding the modelling of the drive control, it is based on cascaded loops for position, velocity and current control. The position control is based on a proportional controller (P) with the aid of a feed-forward (FFV), and the cycle time is of 4ms. The velocity control has a proportional-integral controller (PI) for the motor velocity control. Finally, the current loop is modeled with just the torque constant gain K_t, as it runs with a much quicker cycle time than the velocity and position control loops.

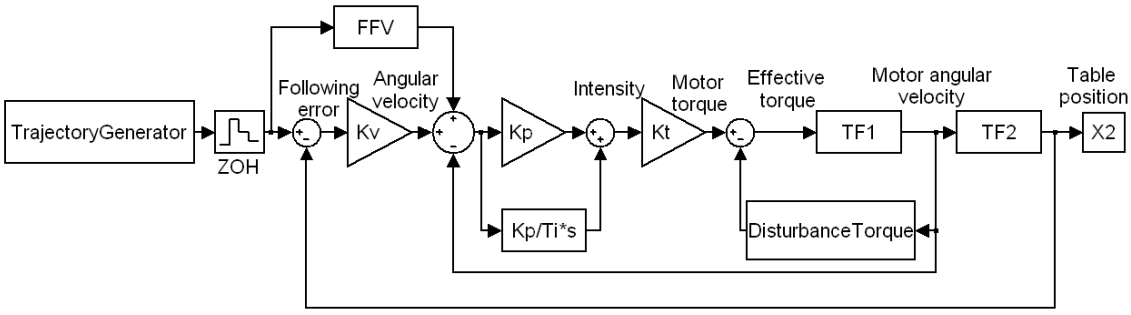

Fig. 2 Mechatronic model of the ballscrew drive in Simulink.

This is a post-peer-review, pre-copyedit version of an article published in The International Journal of Advanced Manufacturing Technology. The final authenticated version is available online at: https://doi.org/10.1007/s00170-017-0597-2

From a mechanical point of view, the dynamics of the drive are modeled after two fundamental transfer functions. The primary transfer function TF_1 relates the torque motor with the angular position of the motor at the encoder. The secondary transfer function TF_2 relates that angular position at the motor with the position of the table measured by the linear encoder. On the other hand, the torque disturbance due to friction has been experimentally identified and modeled.

2.1 Fundamental transfer functions on a 2dof model

The 2 dof model of the ball screw drive testing bench is based on a system of two masses connected by a spring and a damper as it is shown in Fig. 3. This is a well-known approach to the modelling of the dynamics of an electromechanical drive [19], [20]. Here, this model will be set out using natural and modal coordinates to provide a reference for the N dof model.

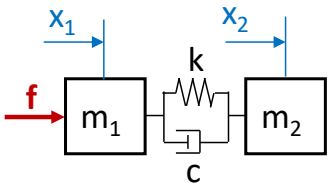

Fig. 3 Lumped parameters model of a2 dof mechanical system.

2.1.1In natural coordinates

The two degrees of freedom of Fig. 3 are the linear position equivalent to the position measurement of the motor encoder and the table position measured at the linear encoder. The first mass represents the motor inertia, and the input force f is equivalent to the motor torque. The second mass represents the inertia of the flexible coupling, screw, nut and table.

$$\begin{bmatrix} m_1 & 0 \\ 0 & m_2 \end{bmatrix} \cdot \begin{Bmatrix} \ddot{x}_1 \\ \ddot{x}_2 \end{Bmatrix} + \begin{bmatrix} c & -c \\ -c & c \end{bmatrix} \cdot \begin{Bmatrix} \dot{x}_1 \\ \dot{x}_2 \end{Bmatrix} + \begin{bmatrix} k & -k \\ -k & k \end{bmatrix} \cdot \begin{Bmatrix} x_1 \\ x_2 \end{Bmatrix} = \begin{Bmatrix} f \\ 0 \end{Bmatrix} \tag{1}$$

There are two modal frequencies where the first one is zero as it is a rigid body mode. The second frequency will be:

$$\omega_2 = \sqrt{\frac{k\left(m_1 + m_2\right)}{m_1 \cdot m_2}} \tag{2}$$

Converting Eq.1 to the Laplace domain, the primary and secondary transfer functions have the following shape:

$$TF_1 = \frac{x_1}{f} = \frac{1}{s^2} \cdot \frac{m_2 s^2 + cs + k}{m_1 m_2 s^2 + \left(m_1 + m_2\right) c \cdot s + \left(m_1 + m_2\right) k} \qquad TF_2 = \frac{x_2}{x_1} = \frac{cs + k}{m_2 s^2 + cs + k} \tag{3}$$

2.1.2Using modal coordinates

The eigenvalue problem of the dynamic matrix of the dynamic model, see Eq.4, provides the modal frequencies as well as the modal matrix [ϕ].

$$\left| \left[K\right] - \omega_i^2 \left[M\right] \right| \left\{\phi_i\right\} = 0 \qquad 1 \le i \le n \tag{4}$$

This is a post-peer-review, pre-copyedit version of an article published in The International Journal of Advanced Manufacturing Technology. The final authenticated version is available online at: https://doi.org/10.1007/s00170-017-0597-2

Normalizing the modal matrix respect to the mass matrix:

$$[\phi]=\begin{bmatrix} \frac{1}{\sqrt{m_1+m_2}} & \sqrt{\frac{m_2}{m_1(m_1+m_2)}} \\ \frac{1}{\sqrt{m_1+m_2}} & -\sqrt{\frac{m_1}{m_2(m_1+m_2)}} \end{bmatrix} \tag{5}$$

In order to convert the motion equation of Eq. 1 to modal coordinates, the coordinates and forces transformation of Eq. 6is performed.

$$\{x\}=[\phi]\cdot\{\delta\} \qquad \{f\}=[\phi]\cdot\{g\} \tag{6}$$

The equation of motion in modal coordinates assuming that proportional damping is:

$$\begin{Bmatrix} \ddot{\delta}_1 \\ \ddot{\delta}_2 \end{Bmatrix}+\begin{bmatrix} 2\cdot\xi_1\cdot\omega_1 & 0 \\ 0 & 2\cdot\xi_2\cdot\omega_2 \end{bmatrix}\cdot\begin{Bmatrix} \dot{\delta}_1 \\ \dot{\delta}_2 \end{Bmatrix}+\begin{bmatrix} \omega_1^2 & 0 \\ 0 & \omega_2^2 \end{bmatrix}\begin{Bmatrix} \delta_1 \\ \delta_2 \end{Bmatrix}=\begin{Bmatrix} g_1 \\ g_2 \end{Bmatrix} \tag{7}$$

The equations of motion are:

$$\ddot{\delta}_1=g_1 \qquad \ddot{\delta}_2+2\xi_2\cdot\omega_2\cdot\dot{\delta}_2+\omega_2^2\cdot\delta_2=g_2 \tag{8}$$

Therefore, the corresponding transfer functions in modal coordinates are:

$$\frac{\delta_1}{g_1}=\frac{1}{s^2} \qquad \frac{\delta_2}{g_2}=\frac{1}{s^2+2\xi_2\cdot\omega_2\cdot s+\omega_2^2} \tag{9}$$

Introducing Eq. 9 in Eq. 6, undoing the conversion to modal coordinates, the following relation between the degrees of freedom and the actuating force is obtained:

$$\begin{aligned} x_1&=\frac{1}{\sqrt{m_1+m_2}}\delta_1+\sqrt{\frac{m_2}{m_1(m_1+m_2)}}\delta_2=\left[\frac{1}{m_t}\cdot\frac{1}{s^2}+\frac{m_2}{m_1\cdot m_t}\cdot\frac{1}{s^2+2\cdot\xi_2\cdot\omega_2\cdot s+\omega_2^2}\right]\cdot f \\ x_2&=\frac{1}{\sqrt{m_1+m_2}}\delta_1-\sqrt{\frac{m_1}{m_2(m_1+m_2)}}\delta_2=\frac{1}{m_t}\left[\frac{1}{s^2}-\frac{1}{s^2+2\cdot\xi_2\cdot\omega_2\cdot s+\omega_2^2}\right]\cdot f \end{aligned} \tag{10}$$

From Eq. 10, the fundamental transfer functions are shown in Eq. 11 as a function of the total mass of the system m_t and the ratio r_m of the second mass m_2 to the motor one m_1.

$$\begin{aligned} TF_1&=\frac{x_1}{f}=\frac{1}{m_t}\cdot\frac{1}{s^2}+\frac{r_m}{m_t}\cdot\frac{1}{s^2+2\xi_2\cdot\omega_2\cdot s+\omega_2^2} \\ TF_2&=\frac{x_2}{x_1}=\frac{2\xi_2\cdot\omega_2\cdot s+\omega_2^2}{(1+r_m)\cdot s^2+2\xi_2\cdot\omega_2\cdot s+\omega_2^2} \end{aligned} \tag{11}$$

Comparing Eq. 11 and Eq.3, using the modal coordinates, the fundamental transfer functions can be obtained in a more explicit way, isolating also the contribution of each mode to the transfer function.

This is a post-peer-review, pre-copyedit version of an article published in The International Journal of Advanced Manufacturing Technology. The final authenticated version is available online at: https://doi.org/10.1007/s00170-017-0597-2

2.2Fundamental transfer functions on a N dof model

Although the 2 dof model can be enough to predict the global dynamic behaviour of the drive [21], N dof lumped parameter models allow analyzing the influence of each component [22]. Here, the following assumptions have been made to develop a 7 dof model of the ball screw drive. The screw shaft is driven with a servomotor connected to a ball screw and nut system via a flexible coupling, see Fig.4. This flexible coupling is divided into two halves, the ring next to the motor and the ring attached to the spindle. The spindle is arranged between two supports with three angular tandem bearings in each one at the extremes of the shaft. The configuration of the two supports of the rotating spindle is a fixed one. These bearings provide radial guiding to the spindle and absorb the forces in the axial direction. To model that configuration, the spindle has been modeled with two springs in parallel that represent the stiffness of either side from the nut.

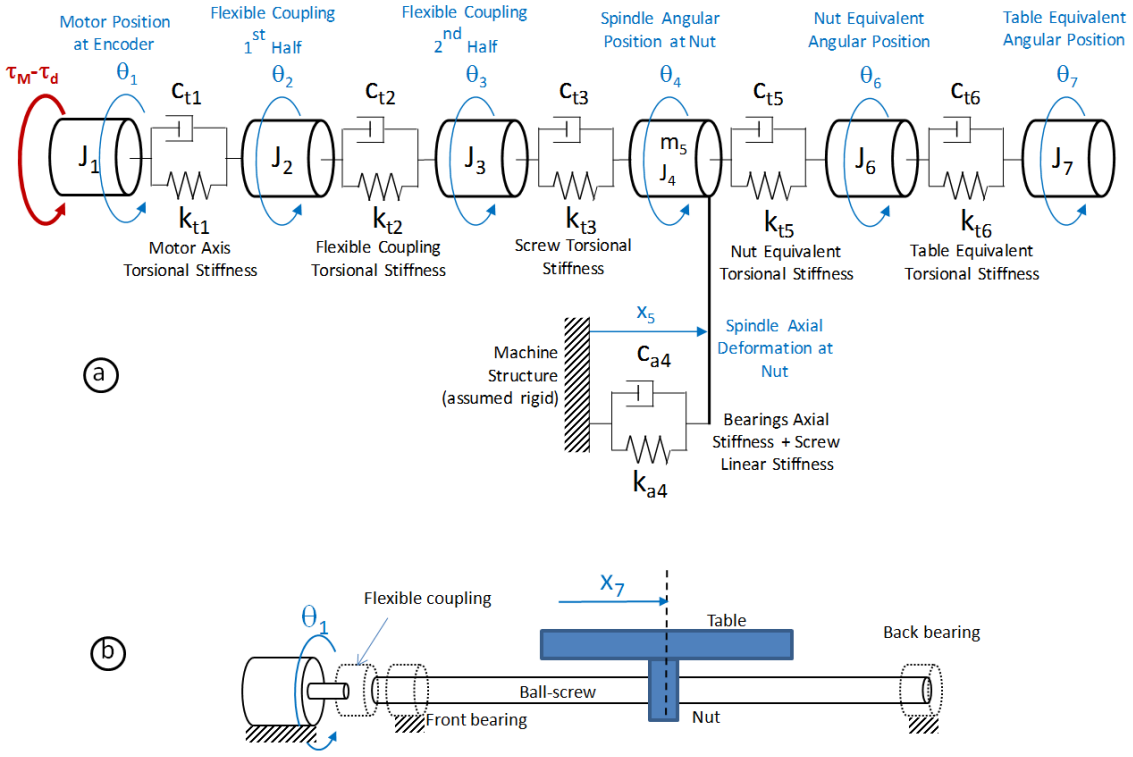

Fig. 4. a) Decoupled model of lumped parameters of 7 dof of a ball screw drive. b) Coupled model.

2.2.1In natural coordinates

In the 7 dof model, six lumped inertias are connected by the corresponding torsional spring and dampers that represent the stiffness and the damping of the transmission chain. The motion is provided by the motor torque τ_M which has to work against the disturbance torque due to the friction τ_d. The resulting torque provides the motion on the drive table x_7, whose angular equivalent is calculated as a function of the screw pitch *p*:

$$\theta_7 = x_7 \frac{2\pi}{p} \tag{12}$$

Hence, the 7 degrees of freedom are: the angular position at the motor encoderθ_1, the angular position at the first ring of the flexible coupling θ_2, the angular position at the second ring θ_3, the

This is a post-peer-review, pre-copyedit version of an article published in The International Journal of Advanced Manufacturing Technology. The final authenticated version is available online at: https://doi.org/10.1007/s00170-017-0597-2

angular position of the screw section at the nut θ_4 as well as its axial deformation x_5, the angular equivalent of the linear position of the nut interface with the table θ_6, calculated as in Eq. 12, and the mentioned angular equivalent of the table linear position at the encoder θ_7.A conversion from linear positions to their equivalent angular ones is done to have a coherent model regarding the units of the degrees of freedom, thus avoiding possible numerical problems. Hence, x5 is also converted to θ_5 following Eq. 12.

Regarding the stiffness of the elements of the transmission chain, it is considered the torsional stiffness of the motor shaft k_{t1}, the flexible coupling k_{t2}, the torsional stiffness of the screw k_{t3} as well as its axial stiffnessk_{a4}together with the axial stiffness of the front and rear bearings, the torsional equivalent of the axial stiffness of the ball screw-nut interface k_{t5}, due to the balls deformation, and the torsional equivalent to the nut and table axial stiffness from the nut interface to the position where the measurement of the linear encoder takes place k_{t6}. Regarding the inertias, it is considered the motor inertiaJ_1, the inertia of the two rings of the flexible coupling J_2 and J_3, the inertia J_4 and mass $m_5$of the screw, the mass of the nut m_6 and table m_7. Again, to have a model coherent in units, all the magnitudes have been converted to their equivalent torsional values at the motor shaft as follows. Also, together with all the springs, several dampers have been introduced to model the structural damping of all the elements.

$$k_{ti} = k_{ai}\left(\frac{p}{2\pi}\right)^2 \qquad J_i = m_i\left(\frac{p}{2\pi}\right)^2 \qquad i = 5,6,7 \tag{13}$$

Thus, the dynamic equations of the drive system can be described and ordered in matrix form, as seen in Eq. 14, where [M], [C] and [K] are the matrices of inertia, damping and stiffness, respectively, and are shown in the Appendix:

$$[J]\{\ddot{q}\}+[C]\{\dot{q}\}+[K]\{q\}=\{\tau\} \tag{14}$$

The τ vector includes the forces and *q* the coordinates of the degrees of freedom, as in Eq. 15.

$$\{\tau\}^T=\{\tau_{ef} \quad 0 \quad 0 \quad 0 \quad 0 \quad 0 \quad 0\} \qquad \{q\}^T=\{\theta_1 \quad \theta_2 \quad \theta_3 \quad \theta_4 \quad \theta_5 \quad \theta_6 \quad \theta_7\} \tag{15}$$

After the conversion to the Laplace domain, all the transfer functions that relate the motion of the degrees of freedom are obtained, see the Appendix. After several operations, the primary and secondary transfer functions to introduce in the mechatronic model of Fig. 2 are represented in Eq. 16. Since they are too long to be represented here explicitly, they appears as a function of the transfer functions that relate the other degrees of freedom.

$$\begin{aligned} TF_1 &= \frac{\theta_1}{\tau} = \frac{1}{\left(J_1 s^2 + c_{t1} s + k_{t1}\right) - \left(c_{t1} s + k_{t1}\right)\cdot TF_{1-2}} \\ TF_2 &= \frac{\theta_7}{\theta_1} = TF_{1-2}\cdot TF_{2-3}\cdot TF_{3-4}\cdot TF_{4-5}\cdot TF_{5-6}\cdot TF_{6-7} \end{aligned} \tag{16}$$

2.2.2Using modal coordinates

The decomposition of the two fundamental transfer functions of Eq. 16 using modal coordinates significantly reduces the computational work during simulation and allows an explicit representation. If the change to modal coordinates of Eq. 6 is applied to the equations of motion of the N dof model like Eq. 4, operating as in Section 2.1.2, the fundamental transfer functions

This is a post-peer-review, pre-copyedit version of an article published in The International Journal of Advanced Manufacturing Technology. The final authenticated version is available online at: https://doi.org/10.1007/s00170-017-0597-2

of a N dof model can be represented explicitly. For 7 dofs, the following primary and secondary transfer functions are obtained:

$$TF_1 = \frac{\theta_1}{\tau} = \sum_{i=1}^{7} \frac{{\phi_{i1}}^2}{s^2 + 2\xi_i \cdot \omega_i \cdot s + {\omega_i}^2}$$
$$TF_2 = \frac{\theta_7}{\theta_1} = \frac{\sum_{i=1}^{7} \left(\frac{\phi_{i7} \cdot \phi_{i1}}{s^2 + 2\xi_i \cdot \omega_i \cdot s + {\omega_i}^2} \right)}{\sum_{i=1}^{7} \left(\frac{{\phi_{i1}}^2}{s^2 + 2\xi_i \cdot \omega_i \cdot s + {\omega_i}^2} \right)} \quad (17)$$

3 Application to a ball screw drive

3.1Inertia and stiffness of the transmission chain elements

To model the stiffness of all the components the theory of elasticity has been used, classified by the standard formulation in Appendix. The inertia and stiffness of each element is classified in Table 1, assuming that the nut is placed in the middle of the spindle shaft. The motor shaft, flexible coupling, ball screw-nut interface and nut rigidities are provided by the manufacturers.

Table 1 Summary of rigidities and inertias of the components

		Stiffness	Inertias and masses
Motor shaft		$k_{t1} = 3,23 \cdot 10^4 \, Nm / rad$	$J_1 = 8,5 \cdot 10^{-4} \, kgm^2$
Flexible coupling		$k_{t2} = 4,01 \cdot 10^3 \, Nm / rad$	$J_2 = J_3 = 8,52 \cdot 10^{-5} \, kgm^2$
	torsion	$k_{t3} = 1,72 \cdot 10^4 \, Nm / rad$	$J_4 = 6,25 \cdot 10^{-4} \, kgm^2$
Screw	axial	$k_{a4} = 1,23 \cdot 10^8 \, N / m$	$m_5 = 5 \, kg$
		$k_{t4} = 311,56 \, Nm / rad$	$J_5 = 1,26 \cdot 10^{-5} \, kgm^2$
Screw-Nut		$k_{a5} = 5,45 \cdot 10^8 \, N / m$	$m_6 = 1,23 \, kg$
		$k_{t5} = 1380,5 \, Nm / rad$	$J_6 = 3,11 \cdot 10^{-6} \, kgm^2$
Nut-Table		$k_{a6} = 6,29 \cdot 10^7 \, N / m$	$m_7 = 68,5 \, kg$
		$k_{t6} = 159,33 Nm / rad$	$J_7 = 1,73 \cdot 10^{-4} \, kgm^2$

In Fig. 5, it is shown the rigid body diagram that represents the working mode of the ball screw spindle and the lumped parameters modelling performed. It is the ball screw section between the front-end bearing and the nut, the one that works at torsion, hence, the ball screw torsional stiffness k_{t3}.

This is a post-peer-review, pre-copyedit version of an article published in The International Journal of Advanced Manufacturing Technology. The final authenticated version is available online at: https://doi.org/10.1007/s00170-017-0597-2

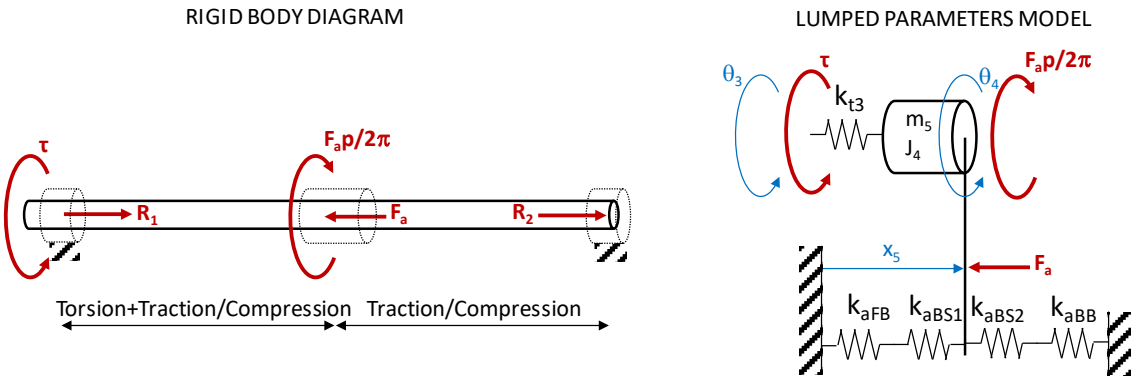

Fig. 5 Working mode of the ball screw spindle and modelling.

On the other hand, to obtain the equivalent axial stiffness of the spindle shaft, it has been considered that, as the two supports are fixed, both sides of the ball screw will work at traction/compression in parallel, hence, k_{aBS1} and k_{aBS2}. Each side will also work in series with the front and back-end bearings axial stiffness, k_{aFB} and k_{aBB}, respectively, so the resultant axial stiffness k_{a4} is:

$$k_{a4} = \frac{k_{aFB} \cdot k_{aBS1}}{k_{aFB} + k_{aBS1}} + \frac{k_{aBB} \cdot k_{aBS2}}{k_{aBB} + k_{aBS2}} \tag{18}$$

The calculation of the stiffness k_{a6} is shown inEq. 19. It considers in series the axial deformation of the nut k_{aN} and the nut support k_{aNS} and the bending of the four screws in parallel that fix the nut support to the table k_{bS}.

$$\frac{1}{k_{a6}} = \frac{1}{k_{aN}} + \frac{1}{k_{aNS}} + \frac{1}{4k_{bS}} \tag{19}$$

3.2 Modes and frequencies

3.2.1 Modes and frequencies in the N dof model

The modal frequencies obtained from the eigenvalue problem of the dynamic matrix are in Hz:

$$\{f_n\}^T = \{0 \quad 144 \quad 432 \quad 870 \quad 2474 \quad 2909 \quad 3900\} \tag{20}$$

The modal matrix, where the eigenvectors are classified by columns:

$$[\phi] = \begin{bmatrix} 0.4082 & -0.1022 & 0.4350 & 0.00041 & -0.0336 & -0.0854 & 0.000061 \\ 0.4082 & -0.1006 & 0.3461 & 0.000087 & 0.1986 & 0.9707 & -0.000909 \\ 0.4082 & -0.0860 & -0.4270 & -0.0025 & 0.9607 & -0.2187 & 0.00287 \\ 0.4082 & -0.0824 & -0.5909 & -0.0028 & -0.1118 & 0.0133 & -0.00479 \\ -5.5\cdot10^{-16} & 0.3095 & 0.2341 & -0.7230 & 0.03295 & -0.0108 & -0.2284 \\ 0.4082 & 0.2954 & -0.3205 & -0.6904 & -0.1508 & 0.04681 & 0.9735 \\ 0.4082 & 0.8843 & 0.0428 & 0.02178 & 0.00052 & -0.000091 & -0.0014 \end{bmatrix} \tag{21}$$

This is a post-peer-review, pre-copyedit version of an article published in The International Journal of Advanced Manufacturing Technology. The final authenticated version is available online at: https://doi.org/10.1007/s00170-017-0597-2

Attending to the eigenvectors amplitudes, as shown in Eq. 21 and more intuitively in the Fig.6 for the three first modes, it is noted that the first mode, as expected, corresponds to the rigid body mode, so all components move in phase but the spindle axial deformation which is near zero. The second mode has mainly an axial behaviour, because of the higher value of the last three lines of the 2nd column. In contrast, the third mode is mainly torsional whereas the other modes are due to coupled torsional and axial vibration.

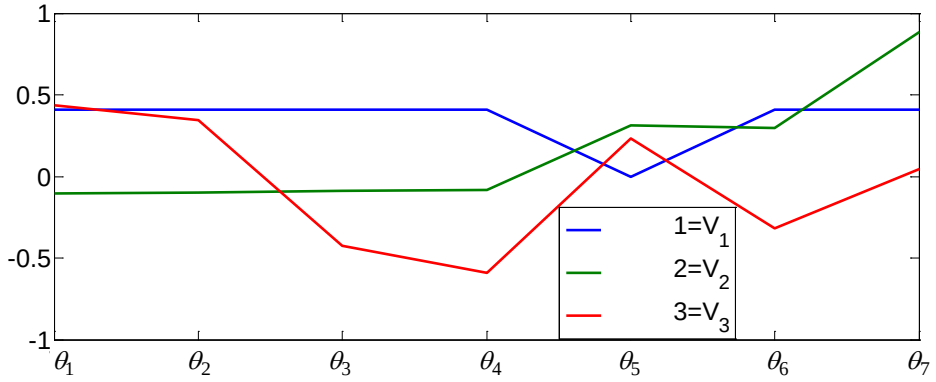

Fig.6 Representation of the first three modes calculated with the 7 dof model.

3.2.2 Modes and frequencies in the 2 dof model

In the 2 dof model, the values of the first and second drive section masses will be calculated as in Eq. 22.

$$m_1 = J_1\left(\frac{2\pi}{p}\right)^2 = 335\ kg \qquad m_2 = m_6 + m_7 + \left(J_2 + J_3 + J_4\right)\left(\frac{2\pi}{p}\right)^2 = 384\ kg \tag{22}$$

Regarding the stiffness, knowing that all rigidities are in series, except the axial and torsional rigidities of the spindle which are arranged in parallel, the equivalent stiffness of the test bench can also be obtained as:

$$k = \frac{1}{\frac{1}{k_{t1}} + \frac{1}{k_{t2}} + \frac{1}{k_{t3} + k_{t4}} + \frac{1}{k_{t5}} + \frac{1}{k_{t6}}} = 5{,}64 \cdot 10^7\ \frac{N}{m} \tag{23}$$

Torsional rigidities of the Eq. 23 have been transformed to their translational equivalent undoing the conversion in Eq. 13. Once the masses and the equivalent stiffness of the system are defined, the natural frequencies have been determined applying Eq. 2, being 0 Hz, the rigid body mode, and 87 Hz.

3.2.3Friction disturbance modelling and identification

A simple friction model with viscous and Coulomb friction has been considered to model the disturbance torque due to the friction.

$$\tau_d = c \cdot \dot{\theta}_1 + \tau_{F_c} \tag{24}$$

This is a post-peer-review, pre-copyedit version of an article published in The International Journal of Advanced Manufacturing Technology. The final authenticated version is available online at: https://doi.org/10.1007/s00170-017-0597-2

The viscous friction coefficient c and Coulomb friction torque τ_{F_c} have been identified experimentally, by measuring torque values at constant feed [23], [24]. Performing a linear regression with the measured torque vs. motor speed, the estimations are c=0.0064 Nms/rad and τ_{F_c} =1.1Nm.

3.3 Results

The 2 and 7dof models have been compared with experimental tests performed in the test bench shown in Fig. 1. In Table2, the parameters and internal variables allocated in the position control and velocity and current regulators are classified. Note that the NC control scheme is represented in Fig. 2.

Table 2 Control gains and parameters

	Featured paremeters	Value of the assigned parameter
P=Proportional controller	K_v	36.841/s
PI =Proportional-integral controller	K_p	20 mA/rpm
	T_i	6.2 ms
Motor torque constant	K_t	1.4 Nm/A

3.3.1Experimental validation in time domain

In the NC of the ball screw test bench, the velocity profile of the path generator takes a square sine shape. In Fig. 7, position, velocity, acceleration, jerk and motor torque of a 100 mm stroke with a feed speed of 7 m/min of feed is shown. The continuous line represents the results from the 7 dof model, the discontinuous line shown the experimental measurements from the linear encoder and the motor, and the commanded position and velocity are also shown by fine solid lines.

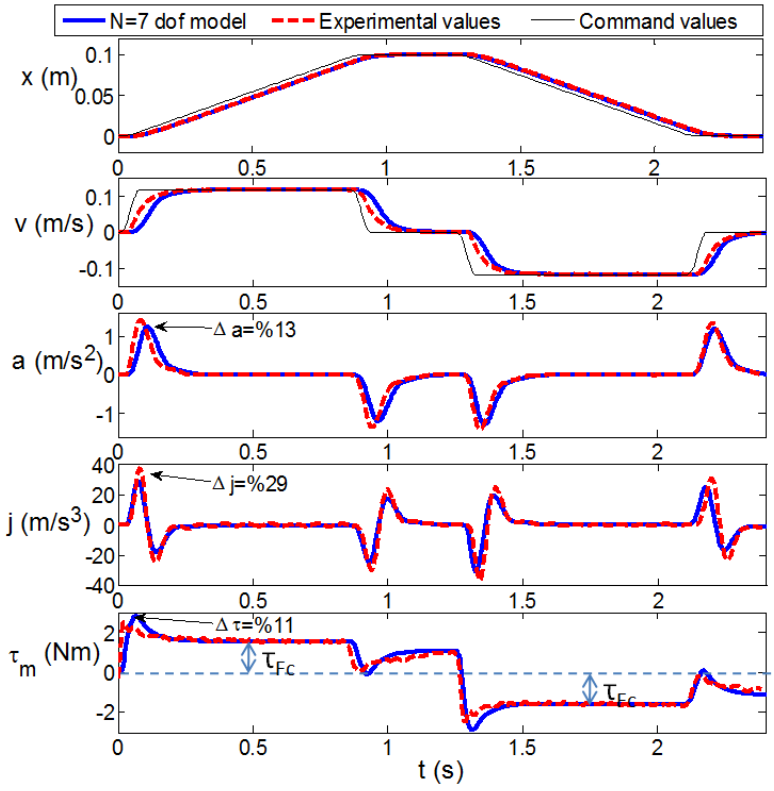

This is a post-peer-review, pre-copyedit version of an article published in The International Journal of Advanced Manufacturing Technology. The final authenticated version is available online at: https://doi.org/10.1007/s00170-017-0597-2

Fig. 7. Comparison 7 dof model vs. experimental measurements: V_f=7 m/min and 100mm stroke.

In Fig. 8, another test is shown. In this case, the motion tested has a stroke of 100 mm and a feed speed of 22 m/min. It can be seen how, for the programmed stroke, the drive spends very little time at constant feed due to the lack of acceleration.

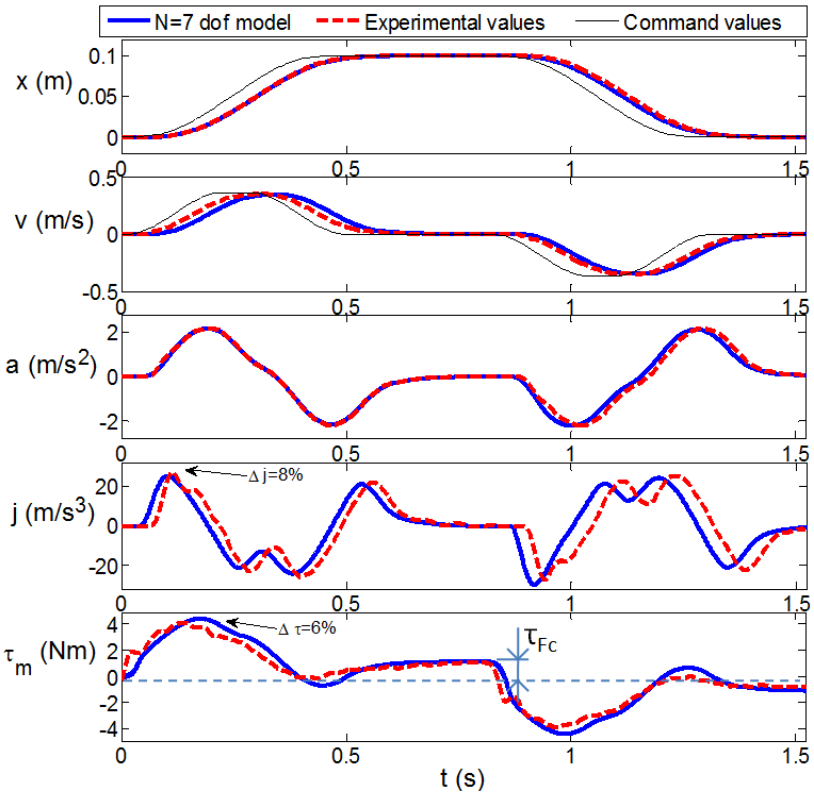

Fig. 8. Comparison 7 dof model vs. experimental measurements: V_f=22 m/min and 100mm stroke.

As can be seen in the Figs. 7 and Fig. 8, the curves of the models and the experimental curves agree reasonably in shape and phase although some deviations are obtained as indicated in the acceleration, jerk and torque peak values. In position the curves of the models are remarkably coincident with the experimental curves. In velocity the amplitudes are remarkably coincident, although for example in Fig. 7 there is a difference in shape probably due to an imprecision in the estimation of damping and friction.

The thicker solid lines represent the values at the output of the drive, i.e. on the table of the drive, reason why its delay in position and velocity respect to the commanded values is logical.

The curves and phases of the experimental and model accelerations coincides very precisely with peaks amplitudes, especially in the case of the Fig. 8 (Vf=22 m/min).

The deviations in the jerk peaks as expected are greater than in acceleration, but shapes and phases are very similar. Although there is a 29% deviation in the jerk peak the result of Fig. 7 of the 7 dof model is correct. The deviation of the maximum value of jerk from Fig. 8 is lower (Δj =

This is a post-peer-review, pre-copyedit version of an article published in The International Journal of Advanced Manufacturing Technology. The final authenticated version is available online at: https://doi.org/10.1007/s00170-017-0597-2

8%), although there is a time delay of the experimental curve, probably due to the problem of setting the common time t=0 for model and experiment.

Finally, the 7 dof model is well coupled to the experimental signals, and although there are deviations in peaks, the magnitude of friction is well estimated as shown in Fig. 7 and Fig. 8. The average torque value due to Coulomb friction in the particular case of 7 m/min (Fig. 7) is 1.59 Nm, and at 22 m/min 1.02 Nm (Fig. 8).

The delays in time can be considered negligible, and the amplitudes of the kinematic and dynamic variables validate well the 7 dof model, therefore, this is very close to the experimental values.

3.3.2Comparison 2 dof model vs. 7 dof model

The2 and 7 dof models are here compared in frequency and time domain. In the frequency domain, it has been compared the Bode diagrams of the primary and secondary transfer functions, and the position closed loop transfer function, table position vs. position command.Fig.9 represents the three Bode diagrams with the main frequencies and the bandwidth of the position closed curves from the 2 and 7 dof models. It is noted that the bandwidth of the position closed loop is the same in the two models, at 2.32 Hz. Furthermore, the variety of resonance peaks in the 7 dof model in comparison with the 2dof model is observed.

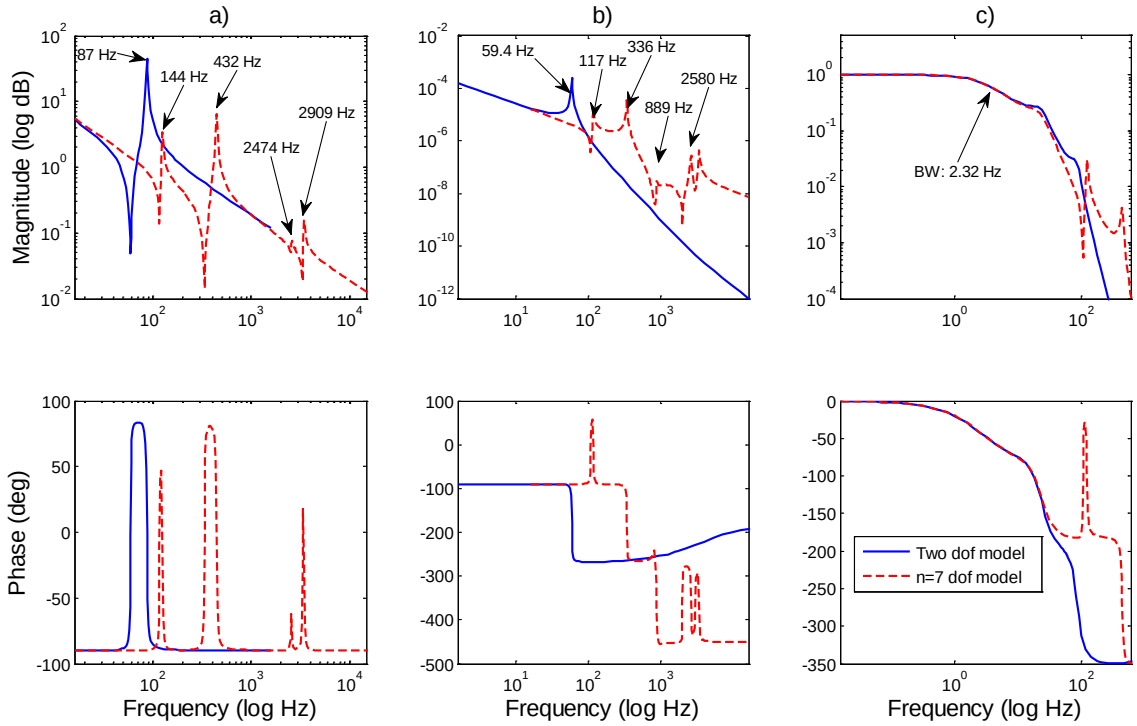

Fig. 9 Frequency domain comparison 2 vs. 7 dof: a) Primary transfer function TF_1, b) Secondary transfer function TF_2, c) Position closed loop transfer function.

A comparison is also performed in time domain in Fig. 10. For a stroke of 100 mm with a feed speed of 30 m/min, it is observed that in position and torque graphic forms coincide except for

This is a post-peer-review, pre-copyedit version of an article published in The International Journal of Advanced Manufacturing Technology. The final authenticated version is available online at: https://doi.org/10.1007/s00170-017-0597-2

some torque oscillations in the 7 dof model. This could be expected since the position closed loop transfer functions are very similar and the dynamic parameters used in both models are the same.

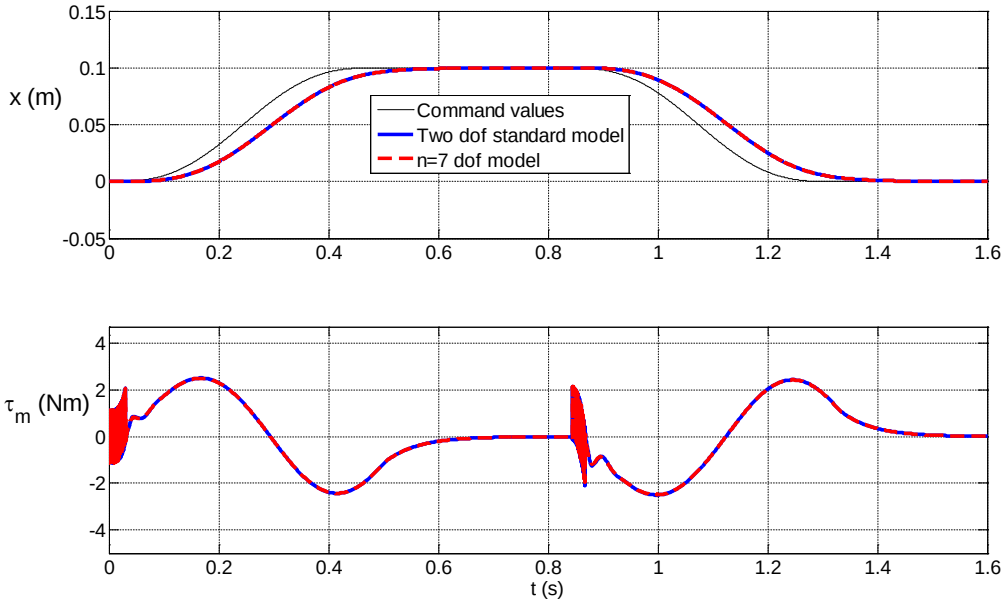

Fig. 10 Time domain comparison 2 dof vs. 7 dof:V_f= 30m/minand100mmstroke.

3.3.3Discussion

Looking at Figs. 7 and 8, it can be said that the 7 dof model predicts the mechatronic behaviour of the ball screw drive accurately. On one hand, attending to the kinematic variables, position, velocity, acceleration and jerk, the model predicts with slight variations the amplitude and the delay of the response of the drive with respect to the programmed path. This implies that the position closed loop calculated and shown in Fig. 10 is in touch with reality, as it conditions the amplitude and delay of the response of the drive.

On the other hand, the calculated torque motor in Figs. 7 and 8 is again close to the experimental one. The shape and amplitude of the signals is very similar, although in the experimental signal there appear some oscillations not identified in the model. Nevertheless, this results imply that the mechatronic model of Fig. 2 with the 7 dof dynamic model used to calculate the primary and secondary transfer functions represents the main phenomena involved in the drive during the motion.

Also, it means that in general it has been done a satisfactory estimation of the dynamic parameters, inertias, masses, stiffness, friction and damping. It must be considered, for example, that the tests were done on purpose moving the drive from the zero position to 100 mm, to check the consistency of the estimation of the spindle torsional stiffness, which was calculated assuming that the nut is at 200 mm, in the middle of the range of the drive. This means that the torsional stiffness during the test has been 2 times or more the used for the model. This fact may be related to the differences in the response delay between the model and the experiments carried out, although, on the other hand, in Fig. 6 it has been demonstrated that the main

limiting mode of the transmission is due to the lack of axial stiffness of the spindle and the nut and table.

Finally, regarding the comparison between the 2 dof model and the 7 dof model, definitely, in time domain and in frequency domain inside the bandwidth there is little difference between both models. Looking at Fig. 6, it is clear that the second mode, the first mode of vibration, is mainly due to the poor axial stiffness of the ball screw spindle and the interface nut-table. That information is of great use in order to redesign the transmission if the bandwidth reached does not meet the requirements, for example, in this case, an axially stiffer spindle and a more robust attachment of the nut to the table would be needed.

The methodology used for this paper corresponds to drives that as a last element in the chain of transmission have a table, another case is that of the drives that in addition to the table move a structural element, such as a column. This structural element adds flexibility to the system, and its influences are developed in the paper by Ansoategui I et al "Influence of the machine tool compliance on the dynamic performance of the servodrives" (2016) [25].

This paper takes into account each element of the drive that can serve for any type of drive ball screw, since the elements are common. This paper has also taken into account the contact between screw-balls-nut. The common elements of the ball screw drive studied are: 1: servomotor, 2. half flexible coupling in the motor side, 3. half flexible coupling in the screw side, 4. screw, 5. nut and 6. table. Each element has its own degree of freedom, but in the case of the axis of the screw have taken into account two displacements: the angular position of the screw in the place of the nut and the degree of freedom that corresponds to the axial deformation of the screw in the location of the nut, since the screw axis is fixed to the bearings of the test bench structure. In total, 7 dof is contemplated.

In order to understand how a greater number of degrees of freedom influence this review, a comparison is made with an paper by Feng G-H et al (2012) [2], which also develops a model of N degrees of freedom. In the paper by Feng G-H et al (2012), the developed parameter set system is 4 dof. There are 4 axes that determine the angular position of the motor, angular position of the ball screw, linear position of the ball screw, and the linear position of the table. The 7 dof model of this paper also contemplates the movement of both halves of the coupling, and the displacement of the nut with respect to the screw axis (screw-ball-nut interference). The modal analysis of Fig. 6 helps to understand more precisely which element of the drive assembly causes greater vibration change.

4 Conclusions

In the present paper a method for the mechatronic modelling and analysis of a ball screw drive has been presented. The main novelty of the model is in the model of the whole mechatronic system, control and dynamics, the two main transfer functions, the primary relating torque and motor velocity and the secondary relating motor and table position, have been obtained using a detailed 7 dof lumped parameters dynamic model. In order to have an efficient computation of such transfer functions, a change to modal coordinates has been implemented so a general

analytical expression of the transfer functions for N dof models has been proposed. The 7 dof model has been compared with a classical 2 dof dynamic model, which is an approach frequently found in the bibliography. Also, several experimental tests have been done on a ball screw drive test bench. The experimental results prove that, after identifying the Coulomb and viscous friction parameters, the position, tracking error, velocity and derivatives and motor torque predicted by the mechatronic model are accurate, both when the 2 dof and the 7 dof models are used. So, it can be concluded that if the objective of the mechatronic model is to simulate the drive dynamic behaviour, a 2 dof model can be enough. However, in order to perform a redesign of the drive or transmission chain, the 7 dof model modal analysis allows identifying the weaker components of the transmission, so any error in the design phase can be virtually identified and corrected before any investment on a first prototype.

References

[1] G. Magnani y P. Rocco, «Mechatronic analysis of a complex transmission chain for performance optimization in a machine tool», *Mechatronics*, vol. 20, n.º 1, pp. 85-101, feb. 2010.

[2] G.-H. Feng y Y.-L. Pan, «Investigation of ball screw preload variation based on dynamic modeling of a preload adjustable feed-drive system and spectrum analysis of ball-nuts sensed vibration signals», *International Journal of Machine Tools and Manufacture*, vol. 52, n.º 1, pp. 85-96, ene. 2012.

[3] S.-T. Wu, S.-H. Lian, y S.-H. Chen, «Vibration control of a flexible beam driven by a ball-screw stage with adaptive notch filters and a line enhancer», *Journal of Sound and Vibration*, vol. 348, pp. 71-87, jul. 2015.

[4] B. Feng, D. Zhang, X. Mei, E. Mu, y X. Huang, «Investigation of the controller parameter optimisation for a servomechanism», *Proceedings of the Institution of Mechanical Engineers, Part B: Journal of Engineering Manufacture*, vol. 229, n.º 1 Suppl, pp. 98-110, feb. 2015.

[5] B. Fernandez-Gauna, I. Ansoategui, I. Etxeberria-Agiriano, y M. Graña, «Reinforcement learning of ball screw feed drive controllers», *Engineering Applications of Artificial Intelligence*, vol. 30, pp. 107-117, abr. 2014.

[6] T. Fujita, A. Matsubara, D. Kono, y I. Yamaji, «Dynamic characteristics and dual control of a ball screw drive with integrated piezoelectric actuator», *Precision Engineering*, vol. 34, n.º 1, pp. 34-42, ene. 2010.

[7] J. Zhang, H. Zhang, C. Du, y W. Zhao, «Research on the dynamics of ball screw feed system with high acceleration», *International Journal of Machine Tools and Manufacture*, vol. 111, pp. 9-16, dic. 2016.

[8] J.-S. Chen, Y.-K. Huang, y C.-C. Cheng, «Mechanical model and contouring analysis of high-speed ball-screw drive systems with compliance effect», *The International Journal of Advanced Manufacturing Technology*, vol. 24, n.º 3-4, jun. 2004.

[9] D. A. Vicente, R. L. Hecker, F. J. Villegas, y G. M. Flores, «Modeling and vibration mode analysis of a ball screw drive», *The International Journal of Advanced Manufacturing Technology*, vol. 58, n.º 1-4, pp. 257-265, may 2011.

[10] L. Zhang, T. Wang, S. Tian, y Y. Wang, «Analytical Modeling of a Ball Screw Feed Drive for Vibration Prediction of Feeding Carriage of a Spindle», *Mathematical Problems in Engineering*, vol. 2016, pp. 1-8, 2016.

[11] L. Dong y W. C. Tang, «Adaptive backstepping sliding mode control of flexible ball screw drives with time-varying parametric uncertainties and disturbances», *ISA Transactions*, vol. 53, n.º 1, pp. 110-116, ene. 2014.

[12] Yamazaki T, «Mathematical model for feed drive system in microscopic motion area», *Archives of Materials Science and Engineering*, vol. 33, pp. 35-38, 2008.
[13] Vesely, J., «Complex model of machine structure with feed drive.», *Int. J of Natural Sciences and Engineering*, vol. 2(4), pp. 193-199, 2009.
[14] Y. Altintas, A. Verl, C. Brecher, L. Uriarte, y G. Pritschow, «Machine tool feed drives», *CIRP Annals - Manufacturing Technology*, vol. 60, n.º 2, pp. 779-796, ene. 2011.
[15] J. J. Zulaika, F. J. Campa, y L. N. Lopez de Lacalle, «An integrated process–machine approach for designing productive and lightweight milling machines», *International Journal of Machine Tools and Manufacture*, vol. 51, n.º 7-8, pp. 591-604, jul. 2011.
[16] H. Ouyang y J. Zhang, «Passive modifications for partial assignment of natural frequencies of mass–spring systems», *Mechanical Systems and Signal Processing*, vol. 50-51, pp. 214-226, ene. 2015.
[17] T. Yang y C.-S. Lin, «Identifying the Stiffness and Damping Parameters of a Linear Servomechanism», *Mechanics Based Design of Structures and Machines*, vol. 32, n.º 3, pp. 283-304, dic. 2004.
[18] Zulaika, Juan José; Ander Altamira, Jon, «Diseño mecatrónico de servomecanismos de alta dinámica», *Automática e instrumentación*, p. (362): 59-64, 5 Ref, 2005.
[19] George Ellis, *Control system design guide.*, 3rd Edition. Elsevier Academic Press, 2004.
[20] GroB, H., Hamann, J., Wiegärtner, G., *Electical feed drives in automation.* Publicis-MCD, 2001.
[21] R. Caracciolo y D. Richiedei, «Optimal design of ball-screw driven servomechanisms through an integrated mechatronic approach», *Mechatronics*, vol. 24, n.º 7, pp. 819-832, oct. 2014.
[22] J. Lee, J. Hyun, S. Wang, y S. Ki, «Development procedure for a vibration transmission element using a reversed design optimization method», *Journal of Sound and Vibration*, vol. 345, pp. 72-85, jun. 2015.
[23] C. L. Chen, M. J. Jang, y K. C. Lin, «Modeling and high-precision control of a ball-screw-driven stage», *Precision Engineering*, vol. 28, n.º 4, pp. 483-495, oct. 2004.
[24] Y.-H. Sun, T. Chen, C. Q. Wu, y C. Shafai, «A comprehensive experimental setup for identification of friction model parameters», *Mechanism and Machine Theory*, vol. 100, pp. 338-357, jun. 2016.
[25] I. Ansoategui, F. J. Campa, C. López, y M. Díez, «Influence of the machine tool compliance on the dynamic performance of the servo drives», *The International Journal of Advanced Manufacturing Technology*, oct. 2016.

Appendix

Mass, stiffness and damping matrices of the 7 dof model

The [M], [K] and [C] matrices in Eq. (12), reduced to the motor shaft, take the following symmetrical form:

This is a post-peer-review, pre-copyedit version of an article published in The International Journal of Advanced Manufacturing Technology. The final authenticated version is available online at: https://doi.org/10.1007/s00170-017-0597-2

$$[J]=\begin{bmatrix} J_1 & 0 & 0 & 0 & 0 & 0 & 0 \\ 0 & J_2 & 0 & 0 & 0 & 0 & 0 \\ 0 & 0 & J_3 & 0 & 0 & 0 & 0 \\ 0 & 0 & 0 & J_4 & 0 & 0 & 0 \\ 0 & 0 & 0 & 0 & m_5\left(\frac{p}{2\pi}\right)^2 & 0 & 0 \\ 0 & 0 & 0 & 0 & 0 & J_6 & 0 \\ 0 & 0 & 0 & 0 & 0 & 0 & J_7 \end{bmatrix}$$

$$[K]=\begin{bmatrix} k_{t1} & -k_{t1} & 0 & 0 & 0 & 0 & 0 \\ -k_{t1} & k_{t2} & -k_{t2} & 0 & 0 & 0 & 0 \\ 0 & -k_{t2} & k_{t2}+k_{t3} & -k_{t3} & 0 & 0 & 0 \\ 0 & 0 & -k_{t3} & k_{t3}+k_{t5} & k_{t5} & -k_{t5} & 0 \\ 0 & 0 & 0 & k_{t5} & k_{a4}\left(\frac{p}{2\pi}\right)^2+k_{t5} & -k_{t5} & 0 \\ 0 & 0 & 0 & -k_{t5} & -k_{t5} & k_{t5}+k_{t6} & -k_{t6} \\ 0 & 0 & 0 & 0 & 0 & -k_{t6} & k_{t6} \end{bmatrix}$$

$$[C]=\begin{bmatrix} c_{t1} & -c_{t1} & 0 & 0 & 0 & 0 & 0 \\ -c_{t1} & c_{t2} & -c_{t2} & 0 & 0 & 0 & 0 \\ 0 & -c_{t2} & c_{t2}+c_{t3} & -c_{t3} & 0 & 0 & 0 \\ 0 & 0 & -c_{t3} & c_{t3}+c_{t5} & c_{t5} & -c_{t5} & 0 \\ 0 & 0 & 0 & c_{t5} & c_{a4}\left(\frac{p}{2\pi}\right)^2+c_{t5} & -c_{t5} & 0 \\ 0 & 0 & 0 & -c_{t5} & -c_{t5} & c_{t5}+c_{t6} & -c_{t6} \\ 0 & 0 & 0 & 0 & 0 & -c_{t6} & c_{t6} \end{bmatrix}$$

Transfer functions of the 7 dof model in natural coordinates

In the following equations, the individual transfer functions between the axes of the components of then dof model in natural coordinatesare shown.

$$TF_1=\frac{\theta_1}{\tau}=\frac{1}{\left[J_1s^2+c_{t1}s+k_{t1}\right]-\left[c_{t1}s+k_{t1}\right]TF_{1-2}}$$

$$TF_{1-2}=\frac{\theta_2}{\theta_1}=\frac{c_{t1}s+k_{t1}}{\left(J_2s^2+\left(c_{t1}+c_{t2}\right)s+\left(k_{t1}+k_{t2}\right)\right)-\left(c_{t2}s+k_{t2}\right)TF_{2-3}}$$

$$TF_{2-3}=\frac{\theta_3}{\theta_2}=\frac{c_{t2}s+k_{t2}}{\left[J_3s^2+\left(c_{t2}+c_{t3}\right)s+\left(k_{t2}+k_{t3}\right)\right]-\left(c_{t3}s+k_{t3}\right)TF_{3-4}}$$

$$TF_{3-4}=\frac{\theta_4}{\theta_3}=\frac{c_{t3}s+k_{t3}}{\left[J_4s^2+c_{t5}s+\left(k_{t3}+k_{t5}\right)\right]+TF_{4-5}\left(c_{t5}s+k_{t5}\right)\left(1-TF_{5-6}\right)}$$

$$TF_{4-5}=\frac{\theta_5}{\theta_4}=\frac{c_{t5}s+k_{t5}}{\left(m_5\left(\frac{p}{2\pi}\right)^2s^2+\left(c_{a4}\left(\frac{p}{2\pi}\right)^2+c_{t5}\right)s+k_{a4}\left(\frac{p}{2\pi}\right)^2+k_{t5}\right)-\left(c_{t5}s+k_{t5}\right)TF_{5-6}}$$

$$TF_{5-6} = \frac{\theta_6}{\theta_5} = \frac{\left(c_{t5}s + k_{t5}\right)\left(\frac{1}{TF_{4-5}} + 1\right)}{\left(J_6 s^2 + \left(c_{t5} + c_{t6}\right)s + k_{t5} + k_{t6}\right) - \left(c_{t6}s + k_{t6}\right)TF_{6-7}}$$

$$TF_{6-7} = \frac{\theta_7}{\theta_6} = \frac{\left(c_{t6}s + k_{t6}\right)}{\left(J_7 s^2 + c_{t6}s + k_{t6}\right)}$$

Equations for stiffness:

Then, equations to determine the values of torsional, axial and bending rigidity are presented. These will be function of the shear modulus G, the torsional moment of inertia J, the bar length L, the Young's modulus E, the area of the cross-section A, and the axial moment of inertiaI.

$$K_{torsional} = \frac{G \cdot J}{L} \qquad K_{axial} = \frac{E \cdot A}{L} \qquad K_{flexure} = \frac{3E \cdot I}{L^3}$$